Applied Physics A (2020) 126:892
https://doi.org/10.1007/s00339-020-04051-x

Applied Physics A
Materials Science & Processing

T.C. : SOLAR ENERGY MATERIALS AND APPLICATIONS

Heat sink/source and chemical reaction in stagnation point flow of Maxwell nanofluid

M. Irfan[1,2] · M. Khan[1] · W. A. Khan[3]

Received: 2 March 2019 / Accepted: 3 October 2020 / Published online: 27 October 2020

Abstract

A modern progress in fluid dynamics has been emphasizes on nanofluids which maintain remarkable thermal conductivity properties and intensify the transport of heat in fluids. Here, the present-day endeavor progresses a Maxwell nanofluid towards stretched cylinder heated convectively. The addition properties, i.e., MHD, stagnation point, thermal radiation, heat sink/source and chemical reactions are elaborated. The homotopic algorithm has been exploited for solutions of ODEs. Here, it is noted that the temperature field enhances for Biot number and radiation parameter. Additionally, Brownian movement and thermophoretic influences have conflicting performance for nanomaterial concentration. The mass transport rate for constructive–destructive chemical reaction is opposite in nature in response to the thermal Biot number. The ratification of our findings is also addressed via tables and attained noteworthy results.

Keywords Maxwell nanofluid · Magnetohydrodynaics (MHD) · Thermal radiation · Convective heat transport · Chemical reaction

Abberivations

u, w	Axial and radial velocity components
z, r	Space coordinates
λ	Relaxation time
ν	Kinematic viscosity
σ	Electrical conductivity
B_0	Magnetic field strength
ρ_f	Fluid density
c_f	Specific heat of fluid
α_1	Thermal diffusivity
$(\rho c)_f$	Heat capacity of fluid
k_1	Thermal conductivity
τ	Effective heat capacity ratio
T,C	Fluid temperature and concentration
T_∞,C_∞	Ambient temperature and concentration
h_f	Heat conversion coefficient
T_f	Fluid temperature
C_w	Surface concentration
D_B, D_T	Brownian and thermophoresis diffusion coefficient
q_r	Radiative heat flux
k^*	Mean absorption coefficient
σ^*	Stefan-Boltzmann constant
Q_1	Heat sink/source parameter
K_r	Reaction rate
U_0, U_∞	Reference velocities
l	Specific length
R	Radius of cylinder
$U(z, r)$	Stretching velocity
η	Dimensionless variable
α	Curvature parameter
β	Deborah number
M	Magnetic parameter
A	Velocities ratio parameter
N_b	Brownian motion parameter
N_t	Thermophoresis parameter
R_d	Radiation parameter
Pr	Prandtl number
γ	Thermal Biot number
δ	Heat sink/source parameter
Le	Lewis number
C_R	Chemical reaction parameter

✉ M. Irfan
mirfan@math.qau.edu.pk

[1] Department of Mathematics, Quaid-I-Azam University, Islamabad 44000, Pakistan

[2] Department of Mathematical Sciences Federal, Urdu University of Arts Sciences and Technology, Islamabad 44000, Pakistan

[3] School of Mathematics and Statistics, Beijing Institute of Technology, Beijing 100081, China

Nu_z	Local Nusselt number
Sh_z	Local Sherwood number
Re_z	Local Reynolds number
f	Dimensionless velocity
θ	Dimensionless temperature
ϕ	Dimensionless concentration
ODEs	Ordinary differential equations
PDEs	Partial differential equations
MHD	Magnetohydrodynamics
HAM	Homotopy analysis method

1 Introduction

Recently, the nanoparticles accumulation to the disreputable liquid, the aspects of nanofluids, together with thermo-physical ones, fluctuate in assessment with those of the disreputable liquid without help. Subject to the sort of application, these dissimilarities might show either an optimistic or a destructive part. The reform of nanofluids thermal conductivity is unique and significant optimistic dissimilarities might lead to an enhancement in heat deletion, signifying the opportunity of exhausting nanofluids as coolant in atomic receptacles, that is, protection structures, crucial coolant and austere calamity mitigation policies. Furthermore, the best collective atomic receptacles everywhere in the domain are pressurized water receptacles that are recycled as a coolant. The accumulation of nanoparticles to water can intensify the serious heat fluctuation confines and accelerate reducing heat in the receptacle core. Nanofluids are colloidal diffusion of nanoparticles in a disreputable fluid with magnitude 1–100 nm and retain a capacity of progressive thermal conductivity. These elements, generally a metallic or metallic oxide, exaggerate conduction and convection quantities, leading to different heat transport outside the coolant. Choi [1] established the notion of nanofluids, and reconsidered this study field with their nanoscale nanotube deferral and metallic atoms. For the former two eras, various scientists studied nanofluids as heat transport fluids in several fields [2-12]. The nanofluids have numerous potential benefits resembling high specific area, high diffusion stability, dipping pushing control, dropping particle blockage and flexible possessions, which comprise thermal conductivity and outward wettability. Villarejo et al. [13] analyzed boron nitride nanofluids and discussed the aspects of solar thermal applications. The attained heat transport coefficient was enhanced under the circumstance of turbulent flow up to 18% utilizing nanofluid. Irfan et al. [14] studied numerically the properties of thermal conductivity in Carreau nanofluid. The transport of heat reduces for Brownian and thermophoresis factors. The magnetic dipole and radiation impact on Eyring–Powell nanofluid with activation energy was reported by Waqas et al. [15].

The stagnation point flows dynamically in considerationof how the wide-ranging flow acts. The fluid gesture near the stagnation area at the front of a blunt-nosed frame, occurring on all dense frames stirring in a fluid is characterized as stagnation point flows. The stagnation region comes across the high pressure, the highest heat transfer and rates of mass deposition. Due to their industrial and engineering worth, in the analysis of physiological fluid dynamics, numerous researchers have considered the dynamics of stagnation flow/heat transport under numerous conditions. The cooling of atomic devices in disaster closure, solar dominant phones unprotected to a current of air, hydrodynamic developments, heat exchangers engaged in a low-velocity atmosphere, etc. are some applications of these flows. The use of the similarity conversion to Navier–Stokes terminologies in the stagnation region has been first considered by Hiemenz [16]. Merkin and Pop [17] analyzed the flow initiated by shrinking/stretching surfaces determined by the Arrhenius kinetics in the stagnation region. The stagnation point flow of radiative Maxwell nanofluid caused by a variable thickness with chemical reaction was studied by Khan et al. [18]. They noted that the velocity field declined for higher Deborah number. The combined phenomena of convective and variable conductivity in the stagnation region of unsteady Carreau nanomaterial was established by Khan et al. [19]. They attained dual solutions in the manifestation of MHD and the heat sink/source. They described that for both solutions, the influence of the unsteadiness parameter displays analogous performance on the velocity field. Additionally, the temperature field enhances both solutions for intensifying values of thermal Biot and Prandtl numbers. Latest studies for diverse sorts of fluids over a stagnation region have been elaborated in Refs [20–24].

To scrutinize the properties of chemically reacting flow of Maxwell nanofluid in the stagnation region considering the thermal aspect of convective and radiation, this work has been elaborated. The MHD and heat sink/source are also addressed. Homotopic algorithms are worked for solutions of ODEs. The graphical and tabular study of influential parameters are

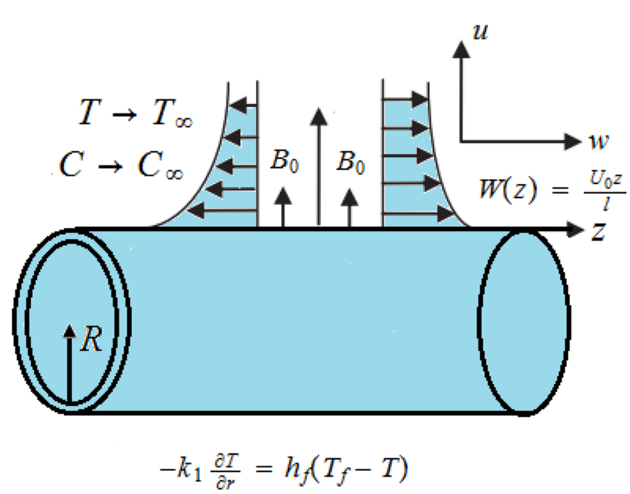

Fig. 1 Schematic diagram

reported. Furthermore, a study compared with a previous work is presented for validation of current outcomes.

2 Mathematical formulation

Here, steady 2D chemically reacting Maxwell nanofluid stagnation point flow of stretching cylinder with radius R has been elaborated. The radiative heat flux, convective heat transport and heat sink/source are also addressed. Furthermore, the mass transport phenomena was reported via chemical reaction. Along the $z-$ direction, the stretching and free stream velocities of the cylinder are reported to be $\left(\frac{U_0 z}{l}, \frac{U_\infty z}{l}\right)$,where l is the specific length and $\left(U_0, U_\infty\right)$ are the reference velocities, respectively. The coordinates of cylindrical surfaces (z, r) considered in such an approach are such that $z-axis$ goes near the axis of the cylinder and $r-axis$ is restrained along the radial direction. The induced MHD is ignored owing to small Reynolds number and B_0 is the length of the magnetic field applied along the $r-$ direction (as plotted in Fig. 1). Thus, the flow problem under these conditions are [25–27]:

$$\frac{\partial u}{\partial r} + \frac{u}{r} + \frac{\partial w}{\partial z} = 0, \tag{1}$$

$$u\frac{\partial w}{\partial r} + w\frac{\partial w}{\partial z} + \lambda\left[w^2\frac{\partial^2 w}{\partial z^2} + u^2\frac{\partial^2 w}{\partial r^2} + 2uw\frac{\partial^2 w}{\partial r \partial z}\right] = W_e\frac{dW_e}{dz} + \nu\left[\frac{\partial^2 w}{\partial r^2} + \frac{1}{r}\frac{\partial w}{\partial r}\right] - \frac{\sigma B_0^2}{\rho_f}\left((W_e - w) + \lambda u\frac{\partial w}{\partial r}\right), \tag{2}$$

$$u\frac{\partial T}{\partial r} + w\frac{\partial T}{\partial z} = \alpha_1\frac{1}{r}\frac{\partial}{\partial r}\left[\left(r\frac{\partial T}{\partial r}\right)\right] + \tau\left[D_B\frac{\partial C}{\partial r}\frac{\partial T}{\partial r} + \frac{D_T}{T_\infty}\left(\frac{\partial T}{\partial r}\right)^2\right] - \frac{1}{(\rho c)_f}\frac{1}{r}\frac{\partial\left(rq_r\right)}{\partial r} + \frac{Q_1(T - T_\infty)}{(\rho c)_f} \tag{3}$$

$$u\frac{\partial C}{\partial r} + w\frac{\partial C}{\partial z} = D_B\frac{1}{r}\frac{\partial}{\partial r}\left(r\frac{\partial C}{\partial r}\right) + \frac{D_T}{T_\infty}\frac{1}{r}\frac{\partial}{\partial r}\left(r\frac{\partial T}{\partial r}\right) - K_r(C - C_\infty), \tag{4}$$

$$w(z, r) = W(z) = \frac{U_0 z}{l},\ u(z, r) = 0,\ -k_1\frac{\partial T}{\partial r} = h_f\left(T_f - T\right),\ C = C_w\, at\, r = R, \tag{5}$$

$$w \to W_e(z) = \frac{U_\infty z}{l},\ T \to T_\infty,\ C \to C_\infty\, as\, r \to \infty. \tag{6}$$

The radiative heat flux q_r is defined as

$$q_r = \frac{-16\sigma^*}{3k^*}T_\infty^3\frac{\partial T}{\partial r}. \tag{7}$$

2.1 Appropriate transformations

Letting

$$u = -\frac{R}{r}\sqrt{\frac{U_0\nu}{l}}f(\eta),\ w = \frac{U_0 z}{l}f'(\eta),\ \theta(\eta) = \frac{T - T_\infty}{T_f - T_\infty}, \quad \phi(\eta) = \frac{C - C_\infty}{C_w - C_\infty},\ \eta = \sqrt{\frac{U_0}{\nu l}}\left(\frac{r^2 - R^2}{2R}\right). \tag{8}$$

Equations (7) and (8) yeild the following ODEs:

$$(1 + 2\alpha\eta)f''' + 2\alpha f'' + ff'' - f'^2 + 2\beta ff'f'' - \beta f^2 f''' - \frac{\alpha\beta}{(1 + 2\alpha\eta)}f^2 f'' - M^2(f' - A - \beta ff'') + A^2 = 0, \tag{9}$$

$$\left(1 + \frac{4R_d}{3}\right)[(1 + 2\alpha\eta)\theta'' + 2\alpha\theta'] + (1 + 2\alpha\eta)\Pr N_b\theta'\phi' + \Pr f\theta' + (1 + 2\alpha\eta)\Pr N_t\theta'^2 + \Pr\delta\theta = 0, \tag{10}$$

$$(1 + 2\alpha\eta)\phi'' + 2\alpha\phi' + Le\Pr f\phi'' + (1 + 2\alpha\eta)\left(\frac{N_t}{N_b}\right)\theta'' + 2\alpha\left(\frac{N_t}{N_b}\right)\theta' - Le\Pr C_R\phi = 0, \tag{11}$$

$$f(0) = 0,\ f'(0) = 1,\ \theta'(0) = -\gamma(1 - \theta(0)),\quad \phi(0) = 1, \tag{12}$$

$$f'(\infty) = A,\ \theta(\infty) = 0,\ \phi(\infty) = 0. \tag{13}$$

The dimensionless quantities are

$$\alpha\left(= \frac{1}{R}\sqrt{\frac{\nu l}{U_0}}\right),\ \beta\left(= \frac{\lambda U_0}{l}\right),\ A = \frac{U_\infty}{U_0},\ M\left(= \sqrt{\frac{\sigma B_0^2 l}{U_0\rho_f}}\right), R_d\left(\frac{4\sigma^* T^3}{kk^*}\right),\ N_b\left(= \frac{\tau D_B(C_w - C_\infty)}{\nu}\right),\ N_t\left(= \frac{\tau D_T(T_f - T_\infty)}{\nu T_\infty}\right),\ \delta\left(= \frac{lQ_0}{U_0(\rho c)_f}\right), \gamma = \left(\frac{h_f}{k_1}\sqrt{\frac{\nu l}{U_0}}\right),\ \Pr\left(= \frac{\nu}{\alpha_1}\right),\ Le\left(= \frac{\alpha_1}{D_B}\right),\ C_R\left(= \frac{K_r l}{U_0}\right). \tag{14}$$

3 Physical quantities of interest

The heat–mass transport quantities (Nu_z, Sh_z) are

$$Nu_z = \frac{-z\left(\frac{\partial T}{\partial r}\right)_{r=R}}{(T_f - T_\infty)},\ Sh_z = \frac{-z\left(\frac{\partial C}{\partial r}\right)_{r=R}}{(C_w - C_\infty)}. \tag{15}$$

In dimensionless form:

Table 1 Outcomes of $-f''(0)$ for β when $\alpha = M = A = 0$

β	$-f''(0)$		
	Abel et al. [28]	Megahed [29]	Present
0.0	1.000000	0.999978	1.000000
0.2	1.051948	1.051945	1.051890
0.4	1.101850	1.101848	1.101849
0.6	1.150163	1.150160	1.150135
0.8	1.196692	1.196690	1.196700
1.2	1.285257	1.285253	1.285360
1.6	1.368641	1.368641	1.368636
2.0	1.447617	1.447616	1.447621

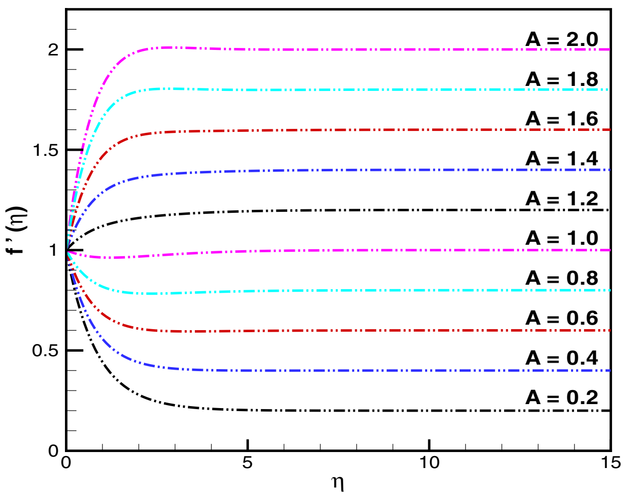

Fig. 2 $f'(\eta)$ for $A < 1$, $A = 1$ and $A > 1$

$$Nu_z \mathrm{Re}_z^{-\frac{1}{2}} = -\left(1 + \frac{4}{3}R_d\right)\theta'(0), \; Sh_z \mathrm{Re}_z^{-\frac{1}{2}} = -\phi'(0), \qquad (16)$$

where $\mathrm{Re}_z = \frac{W(z)z}{\nu}$ depicts the local Reynolds number.

4 Analysis of results

Here, the behavior of radiation, chemical reaction and convective heat transport in the stagnation region for Maxwell nanofluid has been disclosed. For graphical illustrations, the following values of effective parameters are incorporated, i.e., $C_r = 0.2$, $\alpha = \beta = \delta = N_b = 0.3$, $\gamma = N_t = 0.4$, $M = A = 0.5$, $R_d = Le = 1.0$ and $\mathrm{Pr} = 1.5$. Additionally, the confirmation of the current study is established in Table 1. Here, the important fallouts are noted in Refs [28] and [29].

4.1 Graphical depiction of A on $f'(\eta)$

The properties of stagnation point A on fluid velocity are disclosed in Fig. 2. It may be noted that $f'(\eta)$ is magnified when A increases. The differing behavior was documented for both $A > 1$ and $A < 1$ and no effect was noted for $A = 1$. For $A < 1$ a stretching amount outstrips the free stream quantity and the thickness of boundary layer growths. Conversely, the quantity of free stream velocity is advanced when allied with the quantity of stretching velocity when $A > 1$, which decays the thickness of boundary

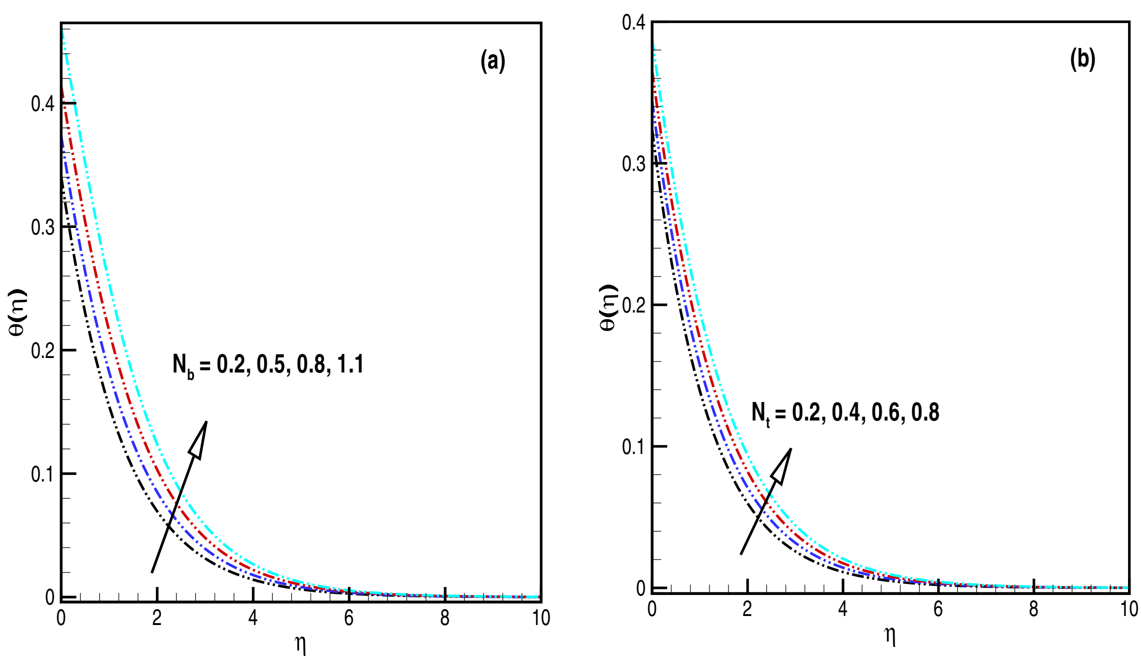

Fig. 3 **a**, **b** $\theta(\eta)$ for (**a**) N_b and (**b**) N_t

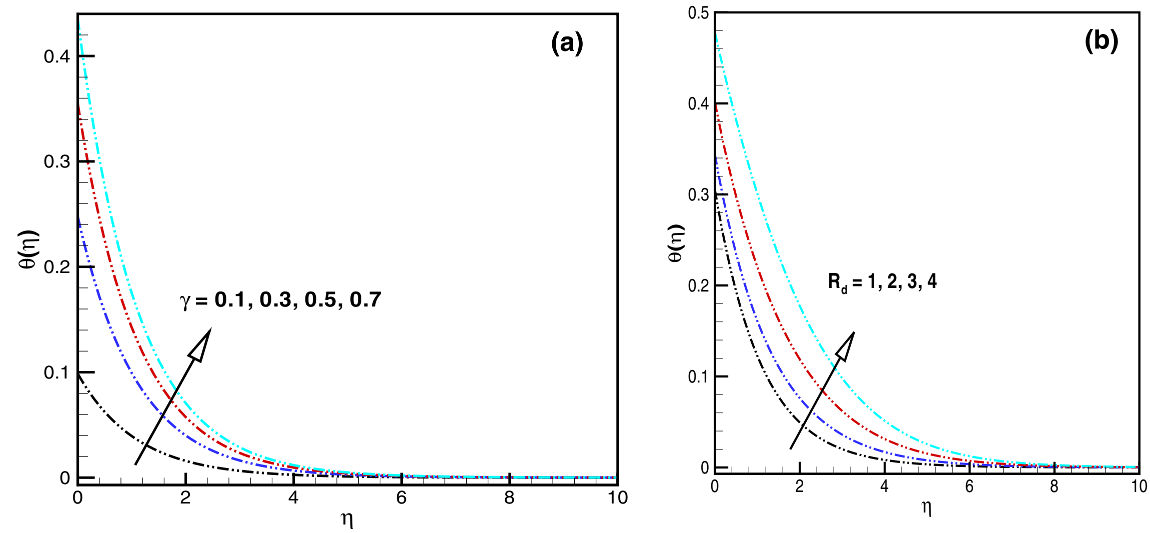

Fig. 4 **a**, **b** $\theta(\eta)$ for (**a**) γ and (**b**) R_d

layer. Moreover, no progress has been acknowledged when $A = 1$; this means that free stream and stretching velocities are analogous.

4.2 Graphical depiction of N_b, N_t, γ and R_d on $\theta(\eta)$.

To portray the characteristics of Brownian N_b and thermophoresis N_t on temperature field, Fig. 3a, b is presented. For N_b and N_t, the increase of the temperature field is detected. The increased values of N_b results in greater Brownian diffusion (D_B), which intensifies the nanofluid temperature due to the direct relation of N_b and D_B. Furthermore, similar is true for N_t. The liquid elements are transported quickly from warm to cold range and increase the theromophoretic force for N_t. Hence,$\theta(\eta)$ is increased for N_t. Figure 4a, b illustrates the depiction of thermal Biot γ and thermal radiation R_d on $\theta(\eta)$. These sketches expose that the temperature increases when γ and R_d increase. The growing values of R_d intensify the surface heat flux which boosts $\theta(\eta)$. Furthermore, the mean absorption factor decreases and the thermal thickness of the layer repeatedly increases. Therefore, $\theta(\eta)$ increases.

4.3 Graphical depiction of C_R, N_b and N_t on $\phi(\eta)$

The effects of chemical reaction parameter C_R, i.e., $C_R < 0$ and $C_R > 0$, on concentration scattering are shown in Fig. 5a, b. The differing nature is acknowledged for $C_R < 0$ and $C_R > 0$. When the values of $C_R < 0$ rise, the concentration field increases; however, the concentration field decays for higher values of $C_R > 0$. Furthermore, the chemical molecular diffusivity fall-offs for $C_R > 0$ and reverse nature are noted for $C_R < 0$. The higher values of Brownian N_b and thermophoretic N_t parameters on $\phi(\eta)$ are plotted as shown in Fig. 6a,b. The concentration fall off for N_b and intensifies for N_t for the Maxwell nanofluid. Physically, N_b increases the unsystematic motion of particles which creates more heat and reduces the Maxwell concentration field. Furthermore, $\phi(\eta)$ rises for N_t. The thermal conductivity of fluid enhances when N_t increases which enhances $\phi(\eta)$.

4.4 Graphical depiction of N_b, N_t and C_R i.e., ($C_R < 0$ and $C_R > 0$) on $Nu_zRe_z^{2}$ and $Sh_zRe_z^{2}$

The graphs of $Nu_zRe_z^{\frac{-1}{2}}$ and $Sh_zRe_z^{\frac{-1}{2}}$ for N_t, N_b and C_R have been reported in Figs. 7a,b; 8a,b. The influence of N_b, and N_t on $Nu_zRe_z^{\frac{-1}{2}}$ causes a decline in performance. The graphs of $Sh_zRe_z^{\frac{-1}{2}}$ for the chemical reaction parameter $C_R < 0$ and $C_R > 0$ are noted to be conflicting. The $Sh_zRe_z^{\frac{-1}{2}}$ decays for higher $C_R < 0$; however, it enhance for $C_R > 0$.

5 Closing remarks

The effect of chemical reaction and radiation on the stagnation point magnetized Maxwell nanofluid is studied. The solution of ODEs via homotpic algorithm (HAM) was exploited. The essential viewpoints are as follows:

The Maxwell temperature field enhanced for larger N_b and N_t

Thermal Biot γ intensified the temperature field.

On concentration field, a relatively opposite performance was noticed for N_b and N_t

Local Sherwood number enhanced for $C_R > 0$ and decayed for $C_R < 0$.

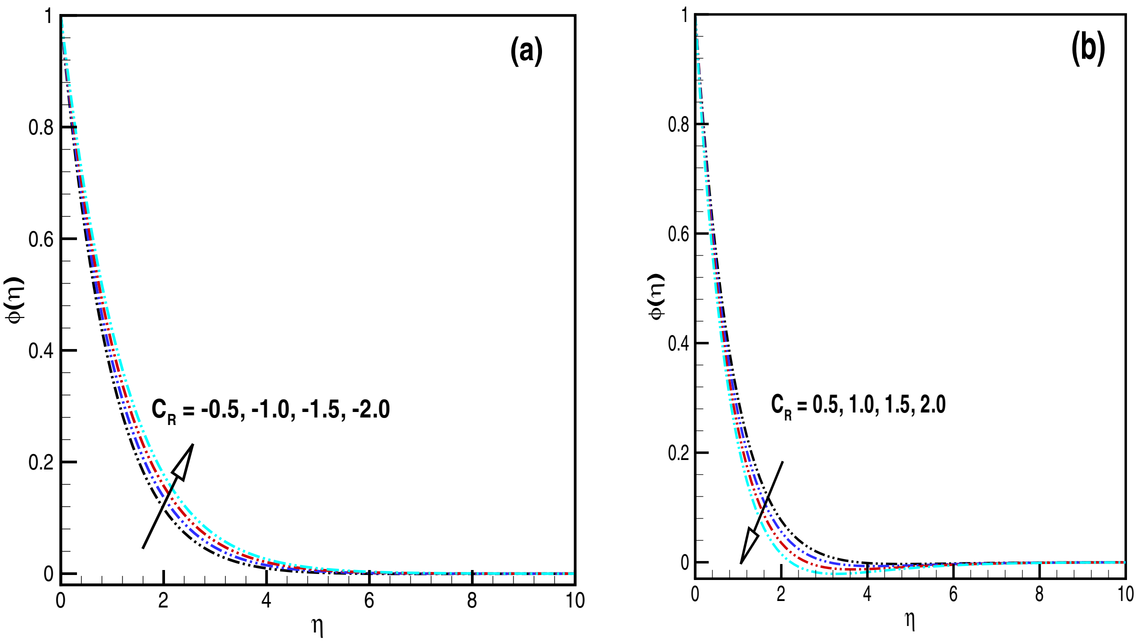

Fig. 5 **a**, **b** $\phi(\eta)$ for (**a**) $C_R < 0$ and (**b**) $C_R > 0$

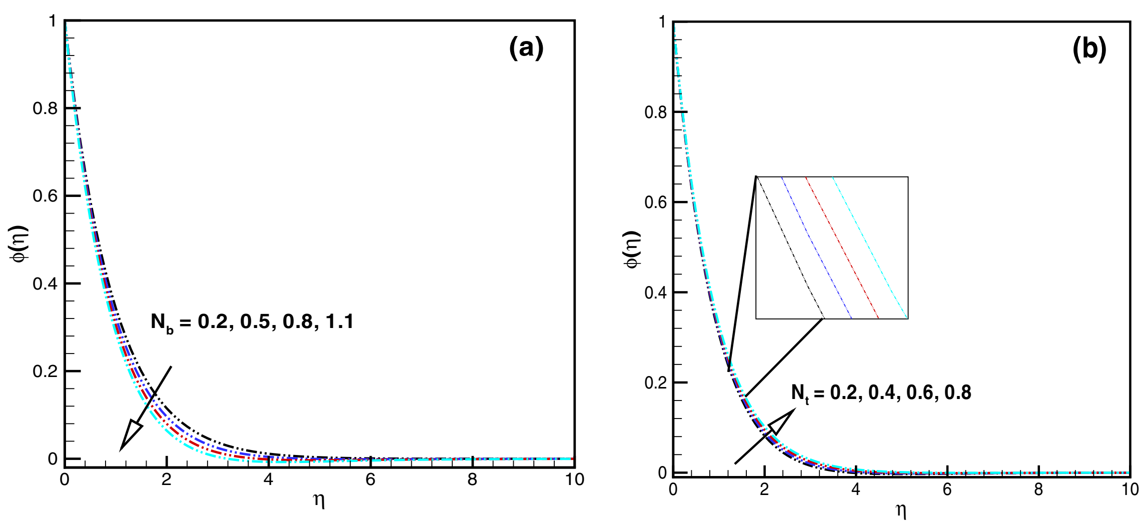

Fig. 6 **a**, **b** $\phi(\eta)$ for (**a**) N_b and (**b**) N_t

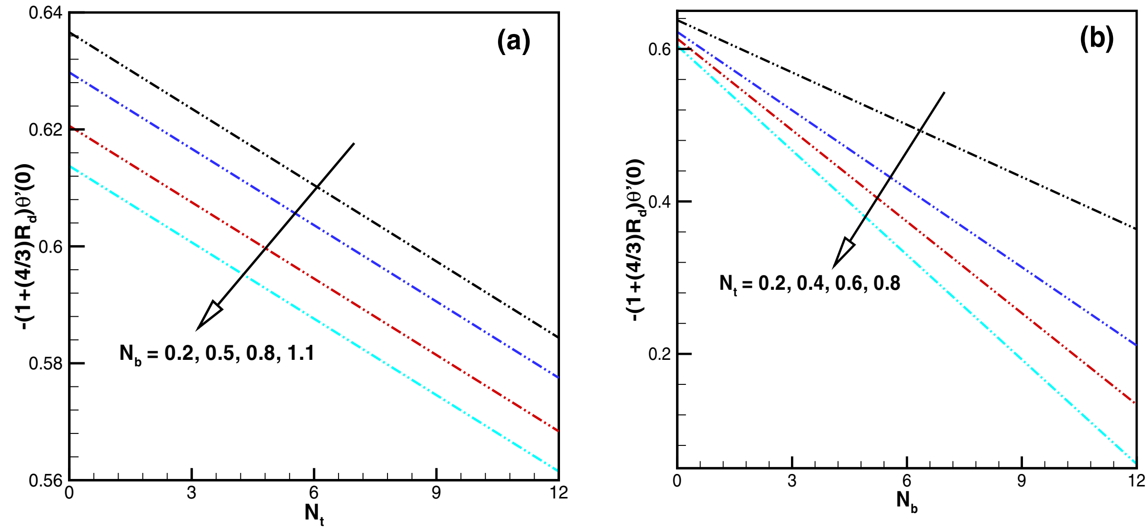

Fig. 7 **a**, **b** $Nu_z Re_z^{\frac{-1}{2}}$ for (**a**) N_b and (**b**) N_t

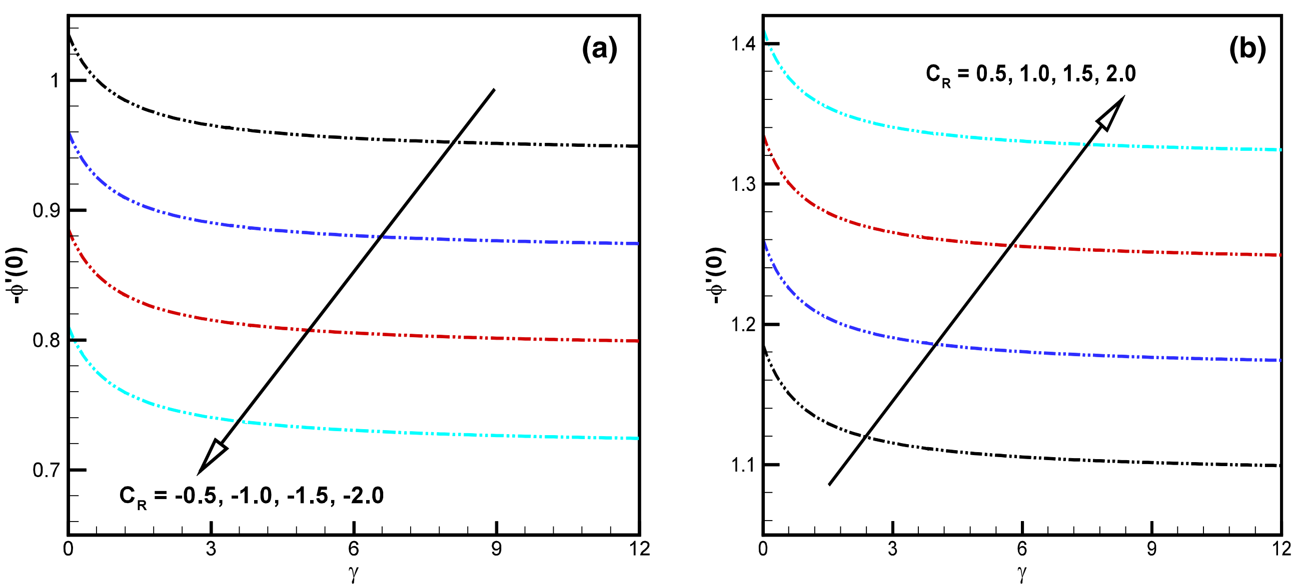

Fig. 8 **a**, **b** $Sh_z Re_z^{\frac{-1}{2}}$ for (**a**) $C_R < 0$ and (**b**) $C_R > 0$

References

1. S.U.S. Choi, Enhancing thermal conductivity of fluids with nanoparticles. ASME Int Mech Eng **66**, 99–105 (1995)
2. H. Masuda, A. Ebata, K. Teramae, N. Hishinuma, Alteration of thermal conductivity and viscosity of liquid by dispersing ultra-fine particles (dispersion of -Al2O3, SiO2 and TiO2 ultra-fine particles). Netsu Bussei **7**, 227–233 (1993)
3. R.U. Haq, Z.H. Khan, S.T. Hussain, Z. Hammouch, Flow and heat transfer analysis of water and ethylene glycol based Cu nanoparticles between two parallel disks with suction/injection ejects. J Mol Liq **221**, 298–304 (2016)
4. S.S. Nourazar, M. Hatami, D.D. Ganji, M. Mhazayinejad, Thermal-flow boundary layer analysis of nanofluid over a porous stretching cylinder under the magnetic field effect. Powder Tech **317**, 310–319 (2017)
5. M. Khan, M. Irfan, W.A. Khan, Impact of nonlinear thermal radiation and gyrotactic microorganisms on the Magneto-Burgers nanofluid. Int J Mech Sci **130**, 375–382 (2017)
6. P.V. Narayana, S.M. Akshit, J.P. Ghori, B. Venkateswarlu, Thermal radiation effects on an unsteady MHD nanofluid flow over a stretching sheet with non-uniform heat source/sink. J Nanofluids **6**, 899–907 (2017)

7. M. Irfan, M. Khan, W.A. Khan, M. Ayaz, Modern development on the features of magnetic field and heat sink/source in Maxwell nanofluid subject to convective heat transport. Phy Lett A **382**, 1992–2002 (2018)
8. R.U. Haq, F.A. Soomro, H.F. Öztop, T. Mekkaoui, Thermal management of water-based carbon nanotubes enclosed in a partially heated triangular cavity with heated cylindrical obstacle. Int J Heat Mass Transf **131**, 724–736 (2019)
9. T.A. Alkanhal, M. Sheikholeslami, M. Usman, R.U. Haq, A. Shafee, A.S. Al-Ahmadi, I. Tlili, Thermal management of MHD nanofluid within the porous medium enclosed in a wavy shaped cavity with square obstacle in the presence of radiation heat source. Int J Heat Mass Transf **139**, 87–94 (2019)
10. R.U. Haq, M. Usman, E.A. Algehyne, Natural convection of CuO–water nanofluid filled in a partially heated corrugated cavity: KKL model approach. Commun Theoretical Phy (2020). https://doi.org/10.1088/1572-9494/ab8a2d
11. H.A. Bafrani, O. Noori-kalkhoran, M. Gei, R. Ahangari, M.M. Mirzaee, On the use of boundary conditions and thermophysical properties of nanoparticles for application of nanofluids as coolant in nuclear power plants; a numerical study. Progress Nuclear Energy **126**, 103417 (2020)
12. R.U. Haq, A. Raza, E.A. Algehyne, I. Tlili, Dual nature study of convective heat transfer of nanofluid flow over a shrinking surface in a porous medium. Int Commun Heat Mass Transf **114**, 104583 (2020)
13. R.G. Villarejo, P. Estell, J. Navas, Boron nitride nanotubes-based nanofluids with enhanced thermal properties for use as heat transfer fluids in solar thermal applications. Solar Energy Mater Solar Cells **205**, 110266 (2020)
14. M. Irfan, K. Rafiq, W.A. Khan, M. Khan, Numerical analysis of unsteady carreau Nanofluid Flow with variable conductivity. Appl Nanosci **10**, 3075–3084 (2020)
15. M. Waqas, S. Jabeen, T. Hayat, S.A. Shehzad, A. Alsaedi, Numerical simulation for nonlinear radiated Eyring-Powell nanofluid considering magnetic dipole and activation energy. Int Commun Heat Mass Transf **112**, 104401 (2020)
16. K. Hiemenz, Grenzschicht an einem in den gleichformigen glussigkeitsstrom einge-tauchten geraden kreiszylinder. Dinglers Polytechnisches J **326**, 321–410 (1911)
17. M.I. Khan, M.I. Khan, M. Waqas, T. Hayat, A. Alsaedi, Chemically reactive flow of Maxwell liquid due to variable thicked surface. Int Commun Heat Mass Transf **86**, 231–238 (2017)
18. J.H. Merkin, I. Pop, Stagnation point flow past a stretching/shrinking sheet driven by Arrhenius kinetics. Appl Math Comput **337**, 583–590 (2018)
19. M. Khan, M. Irfan, L. Ahmad, W.A. Khan, Simultaneous investigation of MHD and convective phenomena on time-dependent flow of Carreau nanofluid with variable properties: dual solutions. Phy Lett A **382**, 2334–2342 (2018)
20. F.U. Rehman, S. Nadeem, H.U. Rehman, R.U. Haq, Thermophysical analysis for three-dimensional MHD stagnation-point flow of nano-material influenced by an exponential stretching surface. Res Phys **8**, 316–323 (2018)
21. B. Mahanthesh, B.J. Gireesha, Dual solutions for unsteady stagnation-point flow of Prandtl nanofluid past a stretching/shrinking plate. Def Diffusion Forum **388**, 124–134 (2018)
22. M. Irfan, M. Khan, W.A. Khan, M. Alghamdi, M. Zaka Ullah, Influence of thermal-solutal stratifications and thermal aspects of non-linear radiation in stagnation point Oldroyd-B nanofluid flow. Int Commun Heat Mass Transf **116**, 104636 (2020)
23. A. Mahdy, A.J. Chamkha, H.A. Nabwey, Entropy analysis and unsteady MHD mixed convection stagnation-point flow of Casson nanofluid around a rotating sphere. Alex Eng J **59**, 1693–1703 (2020)
24. M. Irfan, M. Khan, W.A. Khan, M.S. Alghamdi, Magnetohydrodynamic stagnation point flow of a Maxwell nanofluid with variable conductivity. Commun Theor Phys **71**, 1493–1500 (2019)
25. M. Khan, M. Irfan, W.A. Khan, Heat transfer enhancement for Maxwell nanofluid flow subject to convective heat transport. Pramana J Phy (2018). https://doi.org/10.1007/s12043-018-1690-2
26. M. Khan, M. Irfan, W.A. Khan, Impact of heat source/sink on radiative heat transfer to Maxwell nanofluid subject to revised mass flux condition. Res Phy **9**, 851–857 (2018)
27. M. Rashid, A. Alsaedi, T. Hayat, B. Ahmed, Magnetohydrodynamic flow of Maxwell nanofluid with binary chemical reaction and Arrhenius activation energy. Appl Nanosci **10**, 2951–2963 (2020)
28. M.S. Abel, J.V. Tawade, M.M. Nandeppanavar, MHD flow and heat transfer for the upper-convected Maxwell fluid over a stretching sheet. Meccanica **47**, 385–393 (2012)
29. A.M. Megahed, Variable fluid properties and variable heat flux effects on the flow and heat transfer in a non-Newtonian Maxwell fluid over an unsteady stretching sheet with slip velocity. Chin Phys B **22**, 094701 (2013)